

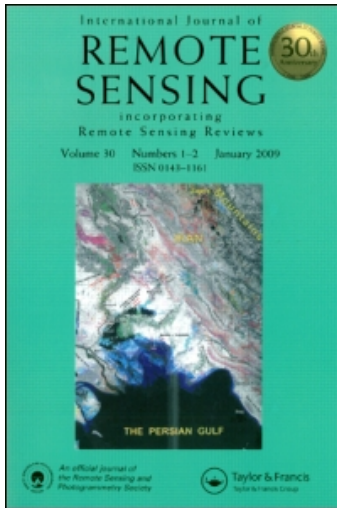
This article was downloaded by: [WALDO - Full Library]

On: 13 September 2010

Access details: Access Details: [subscription number 918522989]

Publisher Taylor & Francis

Informa Ltd Registered in England and Wales Registered Number: 1072954 Registered office: Mortimer House, 37-41 Mortimer Street, London W1T 3JH, UK



International Journal of Remote Sensing

Publication details, including instructions for authors and subscription information:

<http://www.informaworld.com/smpp/title~content=t713722504>

Preliminary and novel estimates of CO₂ gas transfer using a satellite scatterometer during the 2001GasEx experiment

Darek Bogucki^a; Mary-Elena Carr^b; William M. Drennan^a; Peter Woiceshyn^b; Tetsu Hara^c; Marjorie Schmeltz^b

^a RSMAS, University of Miami, Miami, FL, USA ^b Jet Propulsion Laboratory, California Institute of Technology, Pasadena, California, USA ^c Graduate School of Oceanography, University of Rhode Island, Narragansett, Rhode Island, USA

Online publication date: 13 January 2010

To cite this Article Bogucki, Darek , Carr, Mary-Elena , Drennan, William M. , Woiceshyn, Peter , Hara, Tetsu and Schmeltz, Marjorie(2010) 'Preliminary and novel estimates of CO₂ gas transfer using a satellite scatterometer during the 2001GasEx experiment', International Journal of Remote Sensing, 31: 1, 75 – 92

To link to this Article: DOI: 10.1080/01431160902882546

URL: <http://dx.doi.org/10.1080/01431160902882546>

PLEASE SCROLL DOWN FOR ARTICLE

Full terms and conditions of use: <http://www.informaworld.com/terms-and-conditions-of-access.pdf>

This article may be used for research, teaching and private study purposes. Any substantial or systematic reproduction, re-distribution, re-selling, loan or sub-licensing, systematic supply or distribution in any form to anyone is expressly forbidden.

The publisher does not give any warranty express or implied or make any representation that the contents will be complete or accurate or up to date. The accuracy of any instructions, formulae and drug doses should be independently verified with primary sources. The publisher shall not be liable for any loss, actions, claims, proceedings, demand or costs or damages whatsoever or howsoever caused arising directly or indirectly in connection with or arising out of the use of this material.

Preliminary and novel estimates of CO₂ gas transfer using a satellite scatterometer during the 2001 GasEx experiment

DAREK BOGUCKI*[†], MARY-ELENA CARR[‡], WILLIAM M. DRENNAN[†],
PETER WOICESHYN[‡], TETSU HARA[§] and MARJORIE SCHMELTZ[‡]

[†]RSMAS, University of Miami, 4600 Rickenbacker Causeway,
Miami, FL 33149, USA

[‡]Jet Propulsion Laboratory, California Institute of Technology, 4800
Oak Grove Drive, Pasadena, California 91109 USA

[§]Graduate School of Oceanography, University of Rhode Island, 215
South Ferry Road, Narragansett, Rhode Island, USA

(Received 10 October 2007; in final form 7 February 2009)

The ocean takes up approximately 30% of the annual anthropogenic emissions of CO₂. However, the air–sea exchange of carbon dioxide varies by a factor of 2 depending on the formulation of the exchange process. This considerable uncertainty is due in part to the difficulty in parameterizing the gas transfer velocity, k_{660} , usually given as a function of wind speed. Recent field data showed that parametrization using the mean square slope of small scale surface waves provides a more robust strategy to estimate gas transfer (Frew *et al.* 2004). Here we present a preliminary estimation of the gas transfer velocity as a function of upwind Normalized Radar Cross-Section (NRCS) as measured by the scatterometer QuikSCAT. The gas transfer velocity calculated from upwind NRCS exhibits a quadratic-like dependence at low and intermediate wind speeds ($\approx 6 \text{ ms}^{-1}$). This approach represents a promising new tool to obtain global quasi-synoptic estimates of oceanic uptake of CO₂.

1. Introduction

Due largely to the burning of fossil-fuels, the atmospheric concentration of CO₂ has increased by over 30% in the last 150 years. The atmospheric reservoir only holds about half of the annual anthropogenic emissions, since the remainder is taken up by the terrestrial biosphere and by the ocean. The flux of CO₂ between ocean and atmosphere is estimated from the air–sea gradient in partial pressure of CO₂ (Δp_{CO_2}) and an exchange coefficient which depends primarily on the gas transfer velocity, k_{660} , in turn a function of the turbulence of the marine surface boundary layer. The main process controlling the air–sea gas transfer velocity is diffusion across the boundary layer immediately below the ocean surface and at higher wind speeds the transport due to surface breaking waves, i.e. injected bubbles (Zappa *et al.* 2002, Frew *et al.* 2004, Woolf 2005).

The gas transfer velocity is generally parameterized as a function of wind speed; e.g. Nightingale *et al.* (2000). Such wind-based parameterizations attempt to relate gas transfer obtained from deliberate tracer studies, wind tunnel data, and direct covariance flux measurements to wind speed (Liss and Merlivat 1986, Wanninkhof 1992). The different formulations of k_{660} vary by a factor of 2 or more globally. This constitutes a

*Corresponding author. Email: DBogucki@rsmas.miami.edu

major source of uncertainty when quantifying the oceanic sink of CO₂ (Takahashi *et al.* 1997, Feely *et al.* 2001). It is well understood that wind-based parameterizations can only provide an indirect estimate of exchange, because gas transfer is also affected by surfactants, wind fetch, and bubbles, inter alia. However, given the ready availability of model- or satellite-derived wind fields, these formulations have been to date the most viable approach to estimate CO₂ flux on the global scale.

Turbulent fluxes within the marine boundary layer depend on wind speed, but they are also affected by the state of the ocean surface: fetch, swell, and wave age, i.e. whether the sea is fully developed, decaying or growing. Gas is transferred across the air–water boundary when the diffusive sublayer, the thin layer where molecular diffusivity is the dominant process, is disrupted. Experimental studies reveal that the most important process mediating gas transfer at moderate wind speeds is microscale breaking of short wind waves, i.e. those with wavelengths of 0.03–0.1 m (Zappa *et al.* 2002, Bock *et al.* 1999, Peirson and Banner 2003). Recent studies show that the mean wave slope can be used to quantify microscale breaking and gas transfer. In an experimental field study, carried out in coastal environments with highly variable surfactant coverage, the parameterizations of the gas transfer using the mean square slope explained roughly 89–95% of the observed variance in the data; parametrization based on the mean square slope was found to be consistently better than using wind speed (Frew *et al.* 2004).

Guided by these results we have built a simple model of gas transfer based on the observed sea surface roughness from the scatterometer QuikSCAT and applied it to realistic data. We use a quantity that is directly observable by QuikSCAT – the upwind Normalized Radar Cross-Section (NRCS, also referred to as σ_0). Here we use the upwind NRCS to directly derive gas transfer velocity as opposed to the approach where the QuikSCAT NRCS is used to derive a wind speed which is then converted into the gas transfer velocity via one of many formulations (Liss and Merlivat 1986, Wanninkhof 1992, Nightingale *et al.* 2000).

In this paper we use theoretical considerations and a composite sea surface model to evaluate the link between the mean square slope and the observations of NRCS made by QuikSCAT. By comparing nearly concurrent *in situ* gas transfer velocity measured in the second Gas Exchange Experiment, which took place in the equatorial Pacific in February–March 2001 (GasEx 2001), with satellite observations of NRCS we derive a relationship between the *in situ* gas transfer velocity and upwind NRCS.

The GasEx2001 experiment yielded only a few useful data points to test our derived relationship between NRCS and *in situ* gas transfer velocity. Due to a small number of available data points to constrain our derived relationship, a more accurate model and insightful discussion about model differences has to be deferred to a time when more comprehensive data sets are available.

2. The 2001 gas exchange experiment (GasEx 2001)

GasEx 2001 took place in the equatorial Pacific during February–March 2001 (McGillis *et al.* 2004). Funded by NOAA's Office of Global Programs and NSF, GasEx 2001 was a process study aimed at determining the magnitude and controls on the transfer velocity of carbon dioxide in the largest global oceanic source region of CO₂. The principal GasEx platforms were the R/V *Ronald H. Brown* and three buoys. A drogued Air–Sea Interaction Spar (ASIS) buoy (Graber *et al.* 2000) was deployed upon arrival at the study area, while two catamaran buoys, LADAS and the Surface Processes Instrumentation Platform (SPIP), were deployed for short periods from the

R/V *Brown*. The experiment was Lagrangian, with ASIS drifting 7° westward (at 3° S) during the two week deployment. The ship closely followed ASIS except for two regional surveys and a daily disposal run.

The air–sea fluxes used for this study were measured on ASIS using the eddy correlation technique. Data are collected at 20 Hz, and fluxes are calculated every 30 min. A Gill R2A sonic anemometer on the ASIS mast measured the wind vector, which was corrected for platform motion with a full component motion package (Drennan *et al.* 2003). Fluctuations of carbon dioxide and water vapor were measured with an open path LI-COR 7500 infrared gas analyzer, situated 25 cm to the starboard side of the anemometer. The gain of both CO₂ and H₂O channels on the LI-COR tended to drift with time, due to an accumulation of salt on the optics between rain events. This drift was accounted for in the processing by recalibrating the measured humidity signal against references on ASIS and the *Ronald H. Brown*. The same correction factor was applied to the CO₂ channel. Unfortunately a production fault in the LI-COR 7500 rendered the CO₂ data useless during daytime hours due to sunlight contamination, hence only night-time data are used here.

The air–sea flux of CO₂, F_{CO_2} , was calculated from the covariance of the fluctuations of vertical wind velocity and mass concentration of carbon dioxide, taking into account the so-called Webb correction (Webb *et al.* 1980), which accounts for fluctuations in air density (Donelan and Drennan 1995, Fairall *et al.* 2000). Using the GasEx 2001 fluxes from ASIS, and following Sreenivasan *et al.* (1978), we estimate the sampling error of individual CO₂ flux values to be 32%, about twice that recently reported for heat fluxes (Drennan and Shay 2006).

The gas transfer velocity, k_{660} , is calculated from the flux via:

$$k_{660} = \frac{F_{\text{CO}_2}}{\Delta p_{\text{CO}_2}} \cdot L \left(\frac{Sc}{660} \right)^{1/2} \quad (1)$$

where Δp_{CO_2} is the difference in gas concentration in the bulk water, measured with a SAMI-CO₂ sensor (Sunburst Sensors), and the air, measured with LI-CORs both on ASIS and on the *Brown*; see McGillis *et al.* (2004) for details. Sc is the temperature-dependent Schmidt number for carbon dioxide and L is the temperature- and salinity-dependent solubility.

Small-scale wave measurements were made using a scanning laser slope gauge (Bock and Hara 1995) mounted on LADAS. LADAS was deployed for several hours during most evenings, operating under radio control from the *Brown*. The slope gauge yields mean square slope estimates over wavelengths of roughly 0.8–25.1 cm. Wave slope spectra observed during GasEx 2001 are shown in figure 1.

The conditions during GasEx 2001 are discussed by McGillis *et al.* (2004). Winds were steady and easterly, $U_{10\text{m}} = 6.1 \pm 1.3 \text{ ms}^{-1}$, during the two-week deployment period. The wave field was dominated by swell waves from the N-NE, with peak frequencies typically between 0.08 and 0.1 Hz and significant wave heights of $1.7 \pm 0.3 \text{ m}$. The wave age of the wind sea ($c_p/U = 1 \pm 0.1$ or $c_p/u_* = 32 \pm 8$, where c_p is the phase speed at the wind sea peak, and u_* is the friction velocity) is near full development, indicating that the wind waves are in equilibrium with the wind. The energy of the wind-wave field varies with U^4 , consistent with accepted wave growth laws for developed waves, e.g. Kahma and Calkoen (1992).

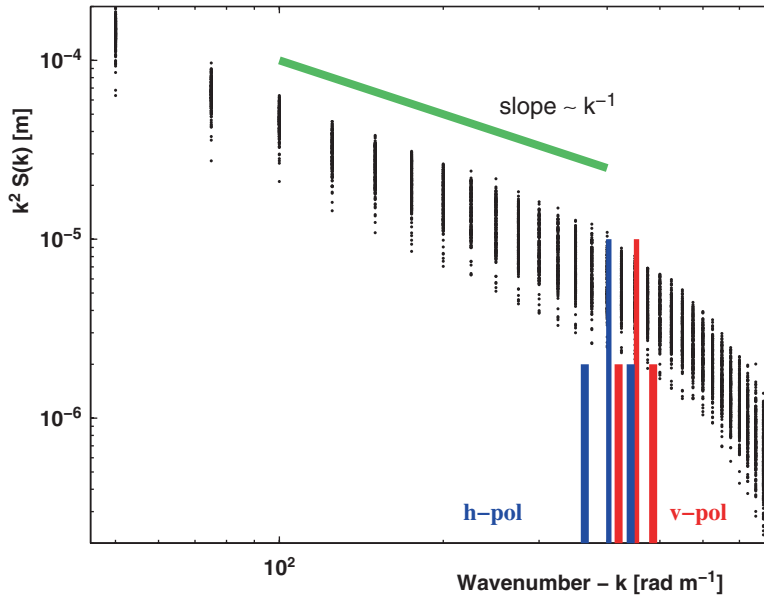


Figure 1. Measured *in situ* omnidirectional wave slope spectra $k^2 S(k)$ collected during the GasEx 2001 experiment between days 45 and 55. The vertical bars correspond to the part of the spectrum sensed by QuikSCAT. The long bars correspond to the central wavenumber of portions of the spectrum that is sensed by QuikSCAT at a given polarization (see the Appendix).

3. QuikSCAT upwind NRCS measurements

The QuikSCAT Ku-band radar (13.46 GHz) signal is particularly sensitive to the ≈ 1.45 cm surface waves which dominate the signal via Bragg scattering. QuikSCAT measures both vertically and horizontally polarized NRCS (*v-pol* and *h-pol* respectively) within the measured swath along the spacecraft path. The radar signal interacts electromagnetically with the ocean surface differently for the two polarizations; the difference depends on both wind speed and sea state. The *h-pol* NRCS measurement has weaker intensity than the *v-pol* at low winds, and the difference decreases with increasing wind speed (Woiceshyn *et al.* 1986). In our procedure we segregate the *v-pol* and *h-pol* NRCS measurements.

QuikSCAT NRCS is related to the short wave slopes of wavelength 1.2–1.8 cm (360 – 510 rad m^{-1}), as shown in the Appendix. QuikSCAT measures a variable number of NRCS values over a single look area within each of the 25 km by 25 km QuikSCAT wind vector cells (WVCs). At higher latitudes, near the poles, QuikSCAT measures up to 80 NRCS values per WVC and this number decreases towards the equator. At the GasEx2001 site typically there were 4 NRCS values per WVC. A detailed description of the QuikSCAT measurement geometry can be found in Perry (2000).

Our upwind NRCS retrieval algorithm takes into account that the NRCS observations of each WVC depend on the relative direction of the antenna and the direction of wave propagation. To remove the effect of varying relative directions, we convert each NRCS to its upwind component, i.e. we estimate the upwind value of each of the multiple NRCS contained within the 50 km radius using the multiple wind vectors within the WVC. Using multiple NRCS within a 50 km radius improves the quality of

upwind estimate for a single NRCS. The upwind estimates are derived using the look-up table (LUT) that empirically relates NRCS with wind speed. The LUT, located at: ftp://podaac.jpl.nasa.gov/pub/ocean_wind/quikscat/model_function, represents a body of calibrated empirical data relating surface wind observations, wind field analysis (from NOAA and ECMWF) for various directions and speeds, and the NRCS measured by scatterometer for various antenna angles, relative azimuth and incidence, and NRCS polarization (Freilich 2003). Two important variables are the incidence angle between nadir and the location of the NRCS footprint and ϕ , the angle between the pointing direction of the scatterometer radar beam and the wind direction. The LUT discretizes incidence angles, relative azimuth angles, and wind speeds by integer increments. We interpolate both wind speed and the azimuth angle, ϕ , to 0.01 increments using Delaunay triangulations to improve on the coarse discriminations of the LUT.

The upwind σ_0 is defined as the NRCS for which the pointing direction of the scatterometer coincides with wind direction, i.e. $\phi = 0$. We have used the original backscatter to wind vector transfer function table (LUT) hence there is no direction convention ambiguity occurring in this process. As an aside, there is very little difference between upwind and downwind backscatter values. The presence of surfactants may, in general, obscure the upwind determination, but these were not observed in significant concentrations during GasEx 2001.

Thus the upwind σ_0 value for each NRCS within the WVC is estimated by choosing the σ_0 closest to the measured NRCS at $\phi = 0$ from the LUT, using the mean wind direction for the WVC, the pointing azimuth direction of the radar beam, and the incidence angle. This approach is the reverse process used to compute the wind vector from the NRCS via LUT tables and suffers from similar errors. Our analysis of the error estimates associated with upwind NRCS yields that upwind NRCS is accurate to within 1 dB in most of the cases. The largest observed uncertainty for the upwind NRCS is around 3 dB.

In general, the upwind NRCS, or σ_0 , is a measure of the roughness of the downwind face of the wave and therefore is independent of the wind-wave geometry. In our data processing we use NRCS data from within a 50 km radius. This final result is a set of NRCS values that are independent of the local wind-wave geometry. We will now relate them to the local wave conditions.

4. Physical significance of QuikSCAT NRCS

The mathematical derivation of the relationship between the upwind QuikSCAT observed NRCS and capillary-gravity wave spectra is presented in the Appendix. Here we present a summary of the physical arguments why the QuikSCAT measured capillary-gravity wave can be related to the gas transfer across the air-sea interface.

Pure gravity waves can be defined practically as those for which the wavelength λ_g exceeds 6 cm while in the case of pure capillary waves, λ_c is less than 2 mm. Surface tension and gravity combine in such a way that the dispersion relation for gravity-capillary waves presents a minimum in phase speed for waves of $\lambda = 1.71$ cm at 20 °C. A consequence of this dispersion relation is that the group velocity for 1 mm capillary waves is equal to the phase speed of 60 cm gravity waves, which in turn allows the two waves to exchange energy. For gravity dominated waves with moderate slopes, the energy flux is towards high wavenumbers, i.e. short capillary waves where the wave energy is transferred ultimately to the near surface currents.

The footprint of the QuikSCAT antenna on the ocean surface has a spatial resolution of 25 km. This represents many wavelengths of the dominant long wave. This means that at every point, QuikSCAT observes a σ_0 which carries averaged information of Bragg dominated waves with the wavelength of $\lambda \approx 1.45$ cm. This wavelength is bounded by two length scales which control respectively the supply and the sink of energy to the capillary waves. Energy supply is related to the fastest growing mode. The fastest growing mode depends on the specific situation (Caponi *et al.* 1991) but in general is given by a wavelength around $\lambda = 1.5\text{--}3$ cm (Csanady 2001). Conversely the sink of energy for capillary waves is given by waves dominated by viscosity, with a wavelength $\lambda_\nu = 2\pi(\nu^2/g)^{1/3} \approx 0.3$ mm, where ν is the viscosity (Zakharov 1991).

As derived in the Appendix, the upwind NRCS observed by QuikSCAT depends to the leading order on the mean wave slopes within the QuikSCAT wavebands 1.2–1.8 cm within the capillary-gravity wave regime. Since the energy of the pure capillary wave component (and the end member of the gravity-capillary-to-capillary waves cascade) is given by $E_{\text{capillary}} = T \cdot (\nabla \xi)^2$ (where T is the surface tension and ξ is the surface displacement), the surface roughness measured by QuikSCAT is in a sense related to the energy ultimately dissipated by the capillary waves. This suggests that short wave slopes measured by QuikSCAT can be a proxy for near-surface energy dissipation and also, consequently, for gas transfer across the air–sea interface.

In the Appendix we derive a relationship between the QuikSCAT observed NRCS and wave slopes with wavenumbers between 360 and 510 rad m^{-1} (equation 23). This relationship has been obtained with a number of simplifying assumptions, chiefly among them: spatially and temporally constant long wave slopes, Gaussian distribution and absence of surfactant, bubbles and sea spray. The absence of significant surfactant concentrations during GasEx was confirmed by *in situ* sampling during the campaign. Significant quantities of bubbles and sea spray are not present at wind speeds encountered during GasEx 2001.

The slopes observed by QuikSCAT come from the wavenumbers between 360 and 510 rad m^{-1} (see Appendix). The field data of Frew *et al.* (2004) for 200–400 rad m^{-1} and 400–800 rad m^{-1} suggest that the wave slopes in the range observed by QuikSCAT should be related to gas transfer speed k_{660} with a linear fit r^2 (percent of variance explained or square of the correlation between the observed values and the values predicted) of at least 85%. Before we match the field observations of gas transfer with QuikSCAT data of the surface wave slopes during GasEx2001 we need to determine which data can be considered co-located and concurrent. The degree of spatial and temporal constancy within the GasEx 2001 field data is discussed below.

5. Spatial and temporal correlation scales

There are very few tight match-ups between the *in situ* GasEx 2001 measurements and QuikSCAT overflights. The value of spatial or temporal correlation scales is indicative of where and when the QuikSCAT measurement can be treated as concurrent and co-located. To have a statistically sound comparison it was necessary to average QuikSCAT observations in space and the *in situ* data in time. This averaging requires care; ideally the time and radius of averaging should only encompass wave fields possessing the same characteristics.

The optimal spatial averaging scale for the wave field was obtained from the autocorrelation function of the swath data. The observed upwind v -*pol* σ_0 values decorrelate after a few hundred km (figure 2A). The autocorrelation function for the

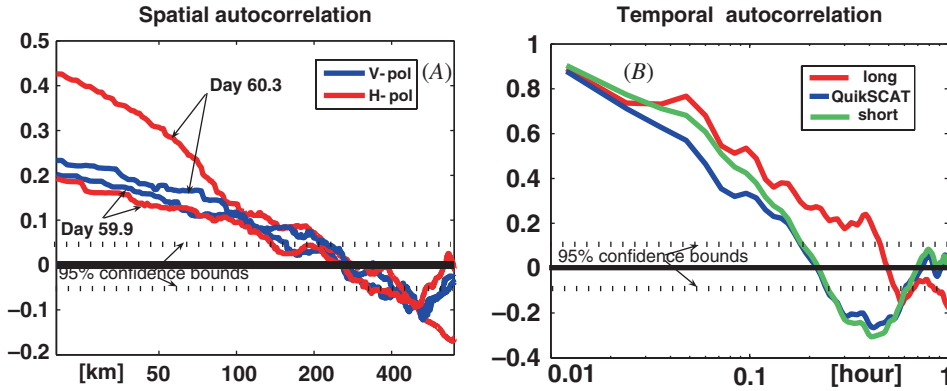


Figure 2. (A) Spatial autocorrelation of σ_0 *v-pol* and *h-pol*. (B) Temporal autocorrelation of spectral slope components from *in situ* data. Note the long wave modulation at, for example, lags of 0.05 and 0.1 hours due to the wavetrains.

h-pol upwind σ_0 decorrelates approximately over the same distance as the *v-pol*. Averaging over a 100 km radius centered on the GasEx site retains the physical processes while maximizing the number of samples.

Similarly the temporal averaging used to improve the statistics should not extend beyond the decorrelation time scale. Representative temporal autocorrelation functions of the *in situ* wave slope data are presented in figure 2(B). We divided the wave field into three components: long waves possessing wavelengths of $O(10\text{ cm})$ or greater, medium waves (denoted QS), corresponding to the QuikSCAT NRCS, with wavelengths of $O(1\text{--}2\text{ cm})$, and the shortest waves possessing wavelengths of $O(1\text{ cm})$ and less. The shortest and QS wave field components decorrelate after $O(0.2\text{ hour})$ while as expected, the long waves decorrelate more slowly $O(0.4\text{ hour})$. Analysis of available GasEx 2001 data used to constrain the model (described in the Appendix), yielded only three data points (k_{660}) within 0.6 hour and 80 km lag and collected nearly concurrently with QuikSCAT passes (QuikSCAT NRCS). Similarly, the sparse *in situ* measurements also led to a two hour lag between the *in situ* wave slope measurement and the QuikSCAT pass, such that the local wave field was decorrelated from its earlier state.

The estimated observed spatial/temporal decorrelation values were used to guide us in selecting the GasEx 2001 data point suitable the model development. In the Appendix, equation (25), we have postulated a relationship between upwind NRCS from QuikSCAT (i.e. $NRCS(\theta_0)$) and the instantaneous spatially averaged wave slopes over QuikSCAT wavebands (i.e. mss_{12}) as: $\log NRCS(\theta_0) = A \log(mss_{12}) + B(\theta_0)$, where the constants A and $B(\theta_0)$ can be determined empirically from *in situ* GasEx 2001 data and the constant $B(\theta_0)$ depends on polarization via the incidence angle θ_0 , i.e. for the *v-pol* $\theta_0 = 0.96$ and for the *h-pol* $\theta_0 = 0.84$. We tested the relationship in equation (25) by comparing the NRCS observed by QuikSCAT and the wave slopes measured *in situ* (figure 3). The three measured points corresponding to nearly concurrent and co-located measurement of waves and NRCS show reasonably good agreement over a decade of wave slopes with the same slope for *v-pol* or *h-pol* (i.e. equal to a constant A which is polarization independent).

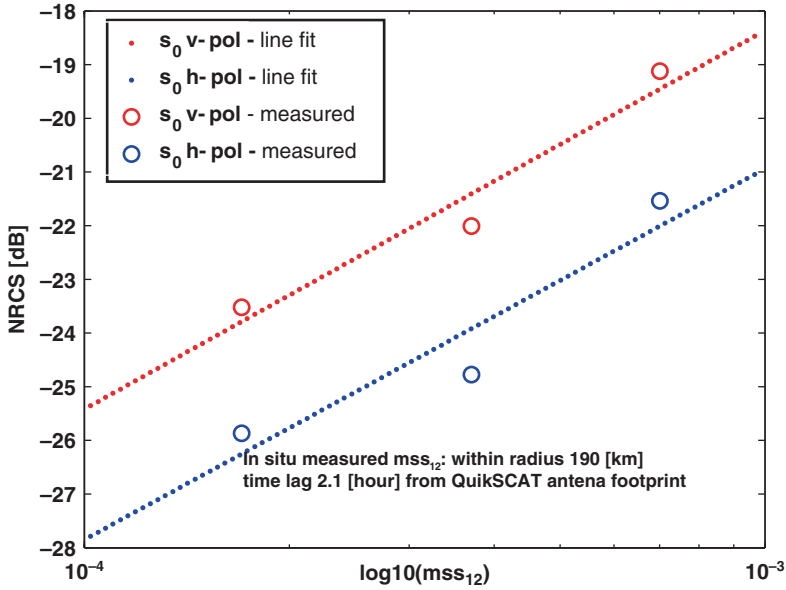


Figure 3. Comparison between observations of the upwind $NRCS(\theta_0)$ measured by QuikSCAT and mean square slopes mss_{12} measured *in situ* at GasEx 2001 and over QuikSCAT wavebands. The measurements are within 2.1 hour and 190 km from QuikSCAT antenna footprint. Note that slopes of the relationship for *v-pol* or *h-pol* are same.

6. Gas transfer velocity from QuikSCAT

The relationship between k_{660} and $NRCS(\theta_0)$ observed by QuikSCAT ideally would be obtained in two steps, first relating $\log(NRCS(\theta_0))$ and $\log(mss_{12})$ and then relating mss_{12} to k_{660} ($mss_{12} \propto k_{660}$) using a large *in situ* database. However the paucity of data acquired during GasEx 2001 led to fewer match-ups between mss_{12} and QuikSCAT observations than between flux and $NRCS(\theta_0)$. Likewise, it was impossible to carry out a concurrent comparison of the three quantities ($NRCS(\theta_0)$ and *in situ* mss_{12} and k_{660}). We propose that the relationship between mss_{12} and upwind $NRCS(\theta_0)$ given in the Appendix or by equation (25) and the existing linear relationship between wave slopes and gas transfer velocity justifies using an empirical relationship between upwind $NRCS(\theta_0)$ and k_{660} :

$$\log k_{660} = C(\theta_0) \log NRCS(\theta_0) + D(\theta_0). \quad (2)$$

In the above, C and D are polarization (θ_0) dependent constants (with C dependence on the polarization much weaker than that of D as suggested by equation (24)). Having postulated a relationship between the upwind cross-section observed by QuikSCAT and the *in situ* gas transfer speed k_{660} , we see how they relate to the observed CO_2 transfer across the ocean surface.

Figure 4 shows the relationship derived from the match-ups of air–sea carbon dioxide flux measurements and concurrent σ_0 from QuikSCAT, following equation (2). The two polarizations reflect different incidence angles, leading to slightly different formulations. Numerically these formulas obtained from GasEx2001 data are:

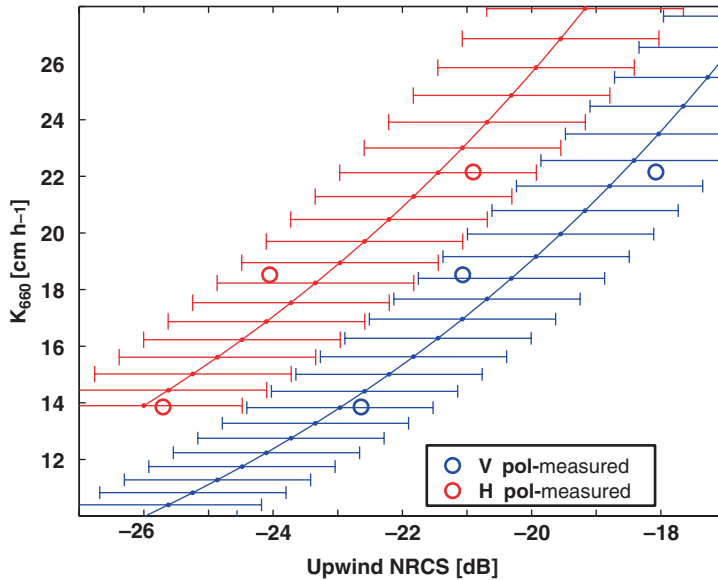


Figure 4. The relationship between upwind σ_0 and the observed *in situ* k_{660} , equation (2); fit within 0.6 hour and 80 km distance from QuikSCAT antenna footprint. The horizontal lines indicate error bars corresponding to 95% confidence levels.

$$k_{660}(\text{cm h}^{-1}) = 10^{(\sigma_{0v} + 47.4079)/21.4248} \quad (3)$$

$$k_{660}(\text{cm h}^{-1}) = 10^{(\sigma_{0h} + 51.7545)/22.5334} \quad (4)$$

for the *v-pol* and *h-pol* respectively; here σ_{0v} and σ_{0h} are the upwind NRCS in dB.

The gas transfer velocity increases linearly with upwind σ_0 , but the increase is greater at greater NRCS, consistent with the enhanced increase in gas exchange at higher wind speeds.

If we assume that the relationship between the observed surface roughness and measured gas transfer velocity derived in the GasEx 2001 study site holds elsewhere, we can use QuikSCAT observations to map the gas transfer velocity. We merged the two polarizations and two different QuikSCAT satellite passes (approximately 12 hours apart) for day 54 of 2001 (24 February) to obtain a regional field of k_{660} (figure 5). On this spatial scale, the data appear ‘blocky’ because of the simplistic merging of the two swaths. Figure 5 presents an expanded view of the study area, the eastern tropical Pacific. Despite steady low winds, the gas transfer velocity varies by a factor of 2 even within the restricted spatial domain of the GasEx 2001 study area (shown as a rectangular box).

As discussed above, gas transfer is most commonly parameterized by wind speed; e.g. Nightingale *et al.* (2000). We can use wind speed to compare our k_{660} value derived from NRCS to the large body of existing experimental CO₂ flux data. The σ_0 -based gas transfer velocity is plotted as a function of concurrent wind speed observed by QuikSCAT in figure 6 and the two polarizations are marked with colors red: *v-pol* and blue: *h-pol*. The slightly different functional dependence of the *v-pol* and the *h-pol* on the wind speed is attributed to different incidence angle and respective sensitivity.

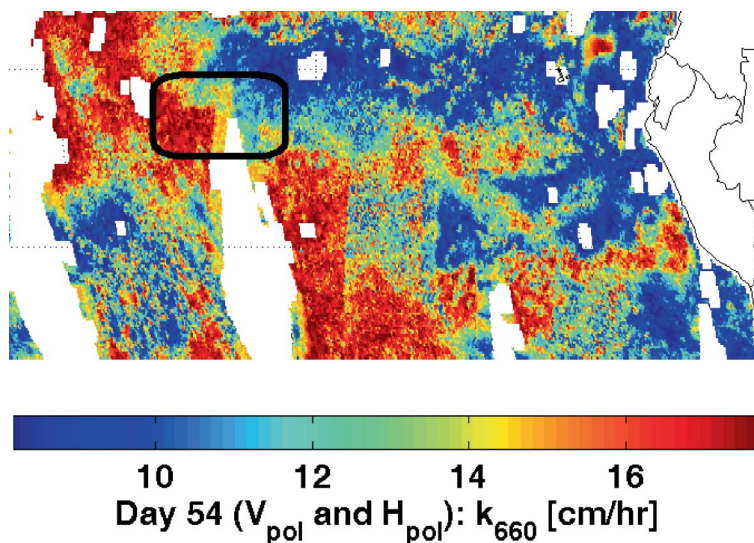


Figure 5. The spatial distribution of k_{660} obtained from both h - pol and v - pol QuikSCAT data in the tropical Pacific for day 54 of 2001 during GasEx 2001. The black rectangle shows the GasEx 2001 study area.

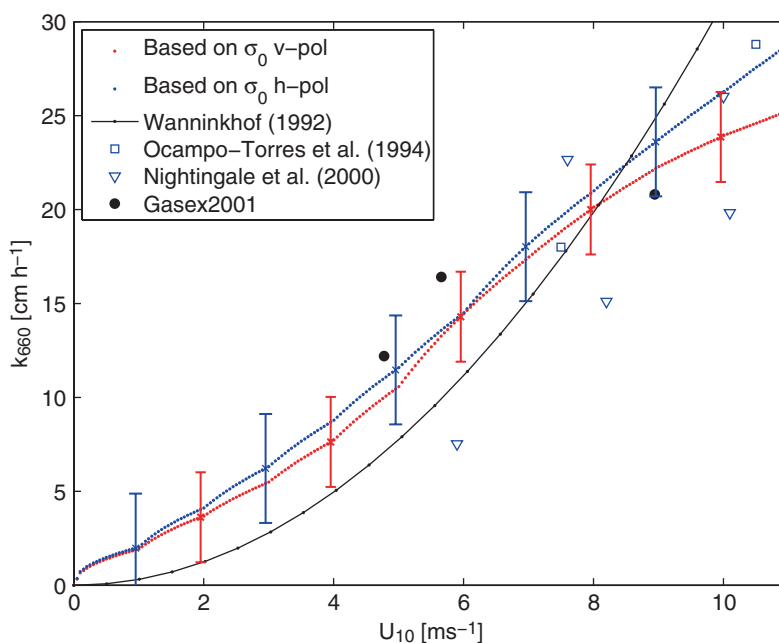


Figure 6. Gas transfer velocity, with associated error bars, obtained from QuikSCAT surface roughness for day 54 of 2001 as a function of concurrent QuikSCAT observations of wind speed (v - pol and h - pol). The curve of Wanninkhof (1992) along with tracer data of Nightingale *et al.* (2000) and laboratory results of Ocampo-Torres *et al.* (1994) are also shown. The solid circles denote the observations collected during the GasEx 2001 experiment.

For wind speeds below 7 m s⁻¹ the relationship is similar to that proposed by Wanninkhof (1992) in which k_{660} is a function of wind speed squared and for winds 7–10 m s⁻¹ consistent with observations of Ocampo-Torres *et al.* (1994) and Nightingale *et al.* (2000).

The prevailing winds in GasEx 2001 were about 6 m s⁻¹. The effect of extrapolation to different wind speeds and associated errors can be seen for winds slower or faster than 6 m s⁻¹ since the *v-pol* and *h-pol* curves begin to diverge at these wind speeds. We speculate that adding data at high wind speeds in future work will decrease the divergence between the curves of the two polarizations and will improve the quality of the overall model. The solid symbols in figure 6 represent the k_{660} measured by QuikSCAT during GasEx 2001 as a function of the wind speed measured by ASIS. The transfer velocities are consistent with those of Nightingale *et al.* (2000), and also with the night-time data from the ship during GasEx (McGillis *et al.* 2004). An important finding from GasEx-2001 was that night-time fluxes (transfer velocities) were found to be enhanced by 40% (30%) over the day-time values. Much of this diurnal variability is not included in k-U relationships, but is accounted for in the k-NRCS relation proposed here.

Our simple model based on three available data points leads to a relatively complex dependence of gas transfer on wind speed which needs to be verified in future experiments that sample a broader range of wind speeds and other environmental conditions.

7. Conclusions

We have developed a new satellite based approach of calculating air–sea gas (CO₂) transfer. We presented a field data set with the measurements needed (fluxes, transfer velocities, short wave slopes, and radar backscatter), to validate the new model. Subsequent analysis of the GasEx 2001 data set (including quality control and analysis of spatial/temporal correlations among wave slopes/CO₂ and the QuikSCAT concurrent/collocated over-passes) yielded a small number of data points available to train the ‘model’. Based on the GasEx 2001 data we have observed that for the eastern tropical Pacific the wave field corresponding to QuikSCAT sensed short waves decorrelates over 100 km and within 0.2 hours.

Based on the derived model we have obtained a relationship between wind speed measured by QuikSCAT and gas transfer velocity estimated from surface roughness as measured by QuikSCAT. Our model relationship indicates a quadratic wind speed dependence of gas transfer speed at intermediate wind speeds, and is consistent with several other independent data sets. The expansion to either lower or higher wind speeds requires more field data.

Acknowledgments

We are grateful to Mark Donelan for his helpful comments. We thank anonymous reviewers for thorough comments on a previous version of this manuscript. WD acknowledges support from NOAA-OGP, grant number NA17RJ1223 and the assistance of Mike Rebozo, Joe Gabriele, and numerous GasEx investigators. DB, MEC, PW, and MS acknowledge the support of the NASA Ocean Biogeochemistry program. Part of this work was carried out at the Jet Propulsion Laboratory under contract with the National Aeronautics and Space Administration. TH acknowledges the support of NOAA CPO/GCC.

References

- BOCK, E. and HARA, T., 1995, Optical measurements of capillary-driven wave spectra using a scanning laser slope gauge. *Journal of Atmospheric and Oceanic Technology*, **12**, pp. 395–403.
- BOCK, J.B., HARA, T., FREW, N.M. and MCGILLIS, W.R., 1999, Relationship between air–sea gas transfer and short wind waves. *Journal of Geophysical Research*, **104**, pp. 25821–25831.
- CAPONI, E.A., YUEN, H.C., MILINAZZO, F.A. and SAFFMAN, P.G., 1991, Water-wave instability induced by a drift layer. *Journal of Fluid Mechanics*, **222**, p. 207.
- CSANADY, G.T., 2001, *Air–sea Interaction: Laws and Mechanisms*, p. 239 (New York: Cambridge University Press).
- DONELAN, M. and DRENNAN, W., 1995, Direct field measurements of the flux of carbon dioxide. In *Proceedings of the Air–water gas transfer*, B. Jähne and E. Monahan (Eds), pp. 677–683 (Hanau: Aeon-Verlag).
- DRENNAN, W.M., GRABER, H.C., HAUSER, D. and QUENTIN, C., 2003, On the wave age dependence of wind stress over pure wind seas. *Journal of Geophysical Research*, **108**(C3), doi 10.1029 / 2000JC000715.
- DRENNAN, W. and SHAY, L., 2006, On the variability of the fluxes of momentum and sensible heat. *Boundary Layer Meteorology*, **119**, pp. 81–107.
- ELFOUHAILY, T., CHAPRON, B., KATSAROS, K. and VANDEMARK, D., 1997, A unified directional spectrum for long and short wind-driven waves. *Journal of Geophysical Research*, **102**, pp. 781–96.
- FAIRALL, C., HARE, J., EDSON, J. and MCGILLIS, W., 2000, Parameterization and micrometeorological measurement of air–sea gas transfer. *Boundary Layer Meteorology*, **96**, pp. 63–105.
- FEELY, R.A., SABINE, C., TAKAHASHI, T. and WANNINKHOF, R., 2001, Uptake and storage of carbon dioxide in the ocean: the global CO₂ survey. *Oceanography*, **14**(4), pp. 18–32.
- FREILICH, M., 2003, SeaWinds Algorithm Theoretical Basis Document. Accessed 23 January 2009. ftp://podaac.jpl.nasa.gov/pub/ocean_wind/quikscat/doc/atbd-sws-01.pdf.
- FREW, N., BOCK, E., SCHIMPF, U., HARA, T., HAUBECKER, H., EDSON, J., MCGILLIS, W., NELSON, R., MCKENNA, S., UZ, B. *et al.*, 2004, Air–sea gas transfer: Its dependence on wind stress, small-scale roughness, and surface films. *Journal of Geophysical Research*, **109**, pp. doi: 10.1029 2003JC002131.
- GRABER, H., TERRAY, E., DONELAN, M., DRENNAN, W., LEER, J.V. and PETERS, D., 2000, A new air–sea interaction spar buoy: design and performance at sea. *Journal of Atmospheric and Oceanic Technology*, **17**, pp. 708–720.
- ISHIMARU, A., 1978, *Wave pPropagation and Scattering in Random Media* (New York: Academic Press).
- JOHNSON, J., TSANG, R. and PAK, K., 1998, A numerical study of the composite surface model for ocean backscattering. *Geoscience and Remote Sensing, IEEE Transactions*, **36**, pp. 72–83.
- KAHMA, K.K. and CALKOEN, C.J., 1992, Reconciling discrepancies in the observed growth of wind-generated waves. *Journal of Physical Oceanography*, **22**, pp. 1389–1405.
- LISS, P.S. and MERLIVAT, L., 1986., Air–sea gas exchange rates: introduction and synthesis. In *The Role of air–sea Exchange in Geochemical Cycling* P.B. Menard (Ed.), pp. 113–129 (Boston: Reidel).
- LIU, Y., YAN, X.H., LIU, W.T. and HWANG, P.A., 1995, The probability density function of ocean surface slopes and its effect on radar backscatter. *Journal of Physical Oceanography*, **27**, pp. 782–790.
- MARCANTONI, D., PIERDICA, N., PULVIRENTI, L. and ZECCHETTO, S., 2005, A joint analysis of radiometric and scatterometric simulations to tune an electromagnetic forward model within a common theoretical framework. *Proceedings of the IEEE International Geoscience and Remote Sensing Symposium, 2005, IGARSS'05*, **4**.
- MCGILLIS, W.R., EDSON, J., ZAPPA, C., WARE, J., MCKENNA, S., TERRAY, E., HARE, J., FAIRALL, C., DRENNAN, W., DONELAN, M., DEGRANDPRE, M., WANNINKHOF, R. and FEELY, R.,

- 2004, air–sea CO₂ exchange in the equatorial Pacific. *Journal of Geophysical Research*, **109**, doi:10.1029/2003JC002256.
- NIGHTINGALE, P., MALIN, G., LAW, C., WATSON, A., LISS, P., LIDDICOAT, M., BOUTIN, J. and UPSTILL-GODDARD, R., 2000, *In situ* evaluation of air–sea gas exchange parameterizations using novel conservative and volatile tracers. *Global Biogeochemical Cycles*, **14**, pp. 373–387.
- OCAMPO-TORRES, F.J., DONELAN, M.A., MERZI, N. and JIA, F., 1994, Laboratory measurements of mass transfer of carbon dioxide and water vapour for smooth and rough flow conditions. *Tellus Series B, Chemical and physical meteorology*, **46**, pp. 16–32.
- PEIRSON, W.L. and BANNER, M.L., 2003, Aqueous surface layer flows induced by microscale breaking wind waves. *Journal of Fluid Mechanics*, **479**, pp. 1–38.
- PERRY, K.L., 2000, *QuikSCAT Science Data Product, User's Manual, Overview and Geophysical Data Products. Version 2.0 Draft, May 2000, D-18053 (JPL)*.
- PHILLIPS, O.M., 1988, Radar Returns from the sea surface - Bragg scattering and breaking waves. *Journal of Physical Oceanography*, **18**, pp. 1065–1074.
- PLANT, W.J., 2003, Microwave sea return at moderate to high incidence angles. *Waves in Random Media*, **13**, pp. 339–354.
- SREENIVASAN, K., CHAMBERS, A.J. and ANTONIA, R.A., 1978, Accuracy of moments of velocity and scalar fluctuations in the atmospheric surface layer. *Boundary Layer Meteorology*, **14**, pp. 341–359.
- TAKAHASHI, T., FEELY, R., WEISS, R., WANNINKHOF, R., CHIPMAN, D., SUTHERLAND, S. and TAKAHASHI, T.T., 1997, Global air–sea flux of CO₂: An estimate based on measurements of sea–air pCO₂ difference. *Proceedings of the National Academy of Sciences U. S. A.*, **94** (16), pp. 8292–8299.
- VALENZUELA, G.R., 1978, Theories for the interaction of electromagnetic and oceanic waves – a review. *Boundary Layer Meteorology*, **13**, pp. 61–85.
- WANNINKHOF, R., 1992, Relationship between wind speed and gas exchange over the ocean. *Journal of Geophysical Research*, **97**, pp. 7373–7382.
- WEBB, E., PEARMAN, G. and LEUNING, R., 1980, Correction of flux measurements for density effects due to heat and water vapour transfer. *Quarterly Journal of the Royal Meteorological Society*, **106**, pp. 85–100.
- WOICESHYN, P., WURTELE, M., BOGGS, D., MCGOLDRICK, L. and PETEHRYCH, S., 1986, The necessity for a new parameterization of an empirical model for wind/ocean scatterometry. *Journal of Geophysical Research*, **91**, pp. 2273–2288.
- WOOLF, D.K., 2005, Parameterization of gas transfer velocities and sea-state-dependent wave breaking. *Tellus B*, **57**, pp. 87–94.
- WRIGHT, J., 1968, A new model for sea clutter. *Antennas and Propagation, IEEE Transactions*, **16**, pp. 217–223.
- ZAKHAROV, V.E., 1991 In *Inverse and Direct Cascade in Wind-Driven Surface Wave Turbulence and Wave-Breaking*, pp. 69–87 (Berlin: Springer-Verlag).
- ZAPPA, C.J., ASHER, W.E., JESSUP, A.T., KLINKE, J. and LONG, S.R., 2002., Effect of microscale wave breaking on air–water gas transfer. In *Gas Transfer at Water Surfaces*, M.A. Donelan, W.M. Drennan, E.S. Saltzman and R. Wanninkhof (Eds), pp. 23–29 (AGU).

Appendix. Relation between upwind QuikSCAT NRCS and small wave slopes

Here we attempt to determine approximately (1) which surface wave spectrum quantity is measured by the QuikSCAT NRCS and (2) which part of the wave spectrum is responsible for the observed QuikSCAT NRCS. To simplify the analysis by removing the dependence of the local wind azimuth angle, we use the NRCS measured by QuikSCAT as converted to their upwind values using the NRCS retrieval algorithm described earlier.

The QuikSCAT footprint is approximately 50 km radius so to obtain the QuikSCAT NRCS from such an area we will need to do some averaging. Throughout the calculations we assume that the ocean surface can be represented by a composite surface model which is the most common model for sea scattered radar return at moderate incidence angles (Wright 1968, Marcantoni *et al.* 2005). The composite surface model is based on the observation that the ocean surface contains a number of spatial scales, ranging from long gravity waves ($O(100\text{ m})$ wavelengths) to short capillary waves ($O(1\text{ mm})$ wavelength).

The composite surface model assumes that scattering can be calculated by dividing the surface wave spectrum into a long wavelength portion and a short wavelength portion for which the SPM (Small Perturbation Method – Bragg scattering for incoherent component) method is used. The split between long and short wave portions is done for waves with wavelengths approximately twice the radar electromagnetic (EM) wavelength (Johnson *et al.* 1998). The numerical simulations of NRCS (Johnson *et al.* 1998) for incidence angles approximately those of QuikSCAT and the QuikSCAT wavenumbers show that the calculated NRCS using SPM combined with a composite surface model and compared to field observations is accurate within a few dB for winds up to 13 ms^{-1} .

7.1 Surface wave spectra

The two dimensional ocean surface is usually represented in terms of the directional wavenumber spectrum ψ such that:

$$\langle \xi^2 \rangle = \int_{-\infty}^{+\infty} \int_{-\infty}^{+\infty} \psi(k_x, k_y) dk_x dk_y = \int_0^{+\infty} \int_{-\pi}^{+\pi} \psi(k, \phi) k dk d\phi = \int_0^{\infty} S(k) dk \quad (5)$$

where the angle bracket $\langle \rangle$ denotes the ensemble average operator, $\langle \xi^2 \rangle$ is the mean square surface displacement, and $S(k)$ is the omnidirectional elevation spectrum such that the total mean square slope is:

$$mss = \langle (\nabla \xi)^2 \rangle = \int_0^{+\infty} S(k) k^2 dk, \quad (6)$$

where $k^2 S(k)$ is the wave slope spectrum. The wave slope spectra observed during GasEx 2001 are shown in figure 1. The mean square slope in the upwind direction mss_x can be expressed as:

$$\begin{aligned} mss_x &= \int_0^{+\infty} \int_{-\pi}^{+\pi} \psi(k, \phi) \cos(\phi) k^3 dk d\phi \\ &= 1/2 \int_0^{+\infty} k^2 S(k) [1 + \Delta(k)/2] \approx 0.6 \int_0^{+\infty} S(k) k^2 dk, \end{aligned} \quad (7)$$

where $\Delta(k)$ is the wavenumber-dependent spreading function. For the wind conditions during GasEx 2001, and for wavenumbers in the range $k = 100\text{--}800\text{ rad m}^{-1}$, the parameter $\Delta(k)$ is constant within 3% and equal to 0.25 (Elfouhaily *et al.* 1997).

7.2 The upwind QuikSCAT NRCS and small wave slopes in the composite surface approximation

To calculate the QuikSCAT NRCS and following Wright (1968) and Marcantoni *et al.* (2005), we assume a composite surface and that the NRCS observed by QuikSCAT is a sum of incoherent contributions, each dominated by Bragg scattering, from local patches of the sea. These patches are geometrically tilted by the underlying gravity waves, which represent the large scale roughness.

The normalized upwind incoherent scattering cross-section due to the short wave component of each patch is determined to the first order (according to SPM) by the resonant Bragg scattering (Valenzuela 1978, Phillips 1988):

$$\sigma_0(k_0) = 16\pi k_0^4 |g_i(\theta_i)|^2 \Psi(2k_0 \sin \theta_i, 0) \quad (8)$$

where $\sigma_0(k_0)$ is the normalized scattering cross-section (non-dimensional quantity) in the upwind direction (the azimuth angle is set to zero), θ_i is the local angle of incidence in the look direction, k_0 is the nominal radar wavenumber for QuikSCAT corresponding to 2.25 cm wavelength, $|g_i(\theta_i)|^2$ is the Fresnel reflection coefficient, and the polarization-dependent subscript i is either *v-pol* or *h-pol*. The function $\Psi(k_x, k_y = 0)$ is the two-dimensional directional folded spectrum of the sea surface displacement, and is related to the directional wavenumber spectrum ψ as $\Psi(k_x, k_y = 0) = 1/2 * [\psi(k_x, k_y = 0) + \psi(-k_x, -k_y = 0)]$ (viewed in the upwind direction $k_y = 0$). In Cartesian coordinates equation (8) can be re-written as (Ishimaru 1978):

$$\sigma_0(k_0) = 16\pi^2 k_0^4 |g_i(\theta_i)|^2 \int_{-\infty}^{\infty} dk_x \int_{-\infty}^{\infty} dk_y \Psi(k_x, k_y) \delta(k_x - 2k_0 \sin \theta_i) \delta(k_y). \quad (9)$$

To simplify the problem we introduce polar coordinates. In these coordinates, transforming the Dirac δ function we get:

$$\sigma_0(k_0) = 16\pi^2 k_0^4 |g_i(\theta_i)|^2 \int_{-\pi}^{\pi} d\phi \int_{-\infty}^{\infty} d\tilde{k} \Psi(\tilde{k}, \phi) \delta(\tilde{k} - 2k_0 \sin \theta_i) \delta(\phi) \quad (10)$$

$$= 16\pi^2 k_0^4 |g_i(\theta_i)|^2 \int_0^{\infty} d\tilde{k} \frac{S(\tilde{k})}{\tilde{k}} \{1 + \Delta(\tilde{k})\} \delta(\tilde{k} - 2k_0 \sin \theta_i) \quad (11)$$

where equation (11) is expressed in polar coordinates such that the azimuth angle $\phi = 0$ is the upwind direction of the omnidirectional elevation spectrum, $S(k)$, and the angular spreading function, $\Delta(k)$ is as given in equation (7).

We will interchangeably express σ_0 or NRCS in decibels, i.e. $NRCS(db) = \sigma_0(dB) = 10 \log_{10}(\sigma_0) = 10 \log_{10}(NRCS)$. The total long wave surface slope S_x relates the local incidence angle θ_i to the nominal incidence angle θ_0 as:

$$\theta_i = \theta_0 - \tan^{-1}(s_x) \simeq \theta_0 - s_x. \quad (12)$$

The last approximation is valid for small slopes such as observed in the GasEx2001 experiment where $s_x = O(0.1)$. Note that we have chosen our sign convention so that $\theta_i < \theta_0$ when $s_x > 0$.

The observed mean upwind long wave slope $\langle s_x^2 \rangle^{1/2}$ for winds of $U_{10m} = 6 \text{ ms}^{-1}$, as observed during GasEx 2001, is around 0.11. The value of the mean long wave slope is much smaller than the nominal incidence angle, θ_0 , which depends on the polarization and assumes either *v-pol* (54° or 0.94 rad) or *h-pol* (46° or 0.8 rad). The slopes s_x thus have the effect of ‘widening’ the Bragg resonance wavenumber by tilting (along the

OX axis) the short waves with respect to the QuikSCAT receiving antenna. This is quantified below.

The range of wavenumbers k that contribute to the NRCS is wider than the narrow-band resonance Bragg wavenumber, $2k_0 \sin \theta_0$ and can be approximated for small slopes as:

$$k = k_0(1 - s_x / \tan(\theta_0)) + O(s_x^2). \quad (13)$$

The Fresnel coefficient for v - pol is given by: $|g_h(\theta_i)|^2 = \cos^4(\theta_i) = [\cos(\theta_0 - s_x)]^4$, and for h - pol : $|g_v(\theta_i)|^2 = [1 + \sin^2(\theta_i)]^2 = [1 + \sin^2(\theta_0 - s_x)]^2$. We change notation of equation (11) by replacing $\sigma_0(k_0)$ with $\sigma_0(s_x; \theta_0)$ to explicitly display σ_0 dependence on the θ_0 (which varies with polarization) and the local upwind long wave slope s_x . We denote $NRCS(\theta_0)$ as an QuikSCAT observed upwind NRCS and explicitly display its polarization dependence on the nominal incidence angle θ_0 .

We introduce the probability, $p(s_x)$, of wave slopes s_x within the large patch area (Marcantoni *et al.* 2005). Then in the composite sea surface approximation the expression for the measured $NRCS(\theta_0)$ becomes (Marcantoni *et al.* 2005):

$$NRCS(\theta_0) = \int_{-\infty}^{\infty} p(s_x) \sigma_0(s_x; \theta_0) (1 - s_x) d(s_x) \simeq \int_{-\infty}^{\infty} p(s_x) \sigma_0(s_x; \theta_0) d(s_x) \quad (14)$$

The factor $(1 - s_x) \simeq 1$ accounts for the change in size of each surface patch when projected along the direction of observation, upwind.

The probability distribution of wave slopes $p(s_x)$ is described by Liu *et al.* (1995). For small wave slopes and small incidence angles $p(s_x)$ becomes Gaussian. It deviates from a Gaussian-like dependence for larger incidence angles and for larger wave slopes.

In addition, in a composite surface approximation, we have divided the whole wave field into Bragg scattering waves and a long wave component. According to numerical simulations (Johnson *et al.* 1998) only the long wave component (usually taken as twice the radar wavelength – waves of 4.4 cm and longer) contributes to the long wave slope distribution $p(s_x)$, in essence filtering short waves out of the $p(s_x)$. We plan in the future, as field data becomes available, to improve our calculation by using more realistic $p(s_x)$.

For simplicity and to allow for comparison with other work (Wright 1968, Johnson *et al.* 1998, Plant 2003, Marcantoni *et al.* 2005) we use here a Gaussian-like dependence given by $p(s_x) = [(2\pi)^{1/2} \sigma_u]^{-1} \exp(-s_x^2 / (2\sigma_u^2))$ with the upwind width of the pdf distribution of large wave slope σ_u to be 0.11 as observed during GasEx 2001.

After substitutions, the upwind $NRCS(\theta_0)$ observed by QuikSCAT becomes:

$$NRCS(\theta_0) = \int_{-\infty}^{\infty} ds_x p(s_x) F_i(s_x; \theta_0) \int_0^{\infty} d\tilde{k} \frac{S(\tilde{k})}{\tilde{k}} \{1 + \Delta(\tilde{k})\} \delta(\tilde{k} - 2k_0 \sin \theta_0 - 2s_x k_0 \cos \theta_0). \quad (15)$$

where $F_i(s_x; \theta_0) = 16\pi^2 k_0^4 |g_i(\theta_i)|^2$. Changing the order of integration, and substituting: $p(s_x)$ ($p(s_x)$ is a symmetric function), $\tilde{k}_1 = 2k_0 \cos \theta_0$ and $\tilde{k}_0 = 2k_0 \sin \theta_0$ (the Bragg wavenumber) we get:

$$NRCS(\theta_0) = \frac{2}{\tilde{k}_1} \int_0^{\infty} d\tilde{k} \frac{S(\tilde{k})}{\tilde{k}} \frac{\exp\{-(\tilde{k} - \tilde{k}_0)^2 / 2(\sigma_u \tilde{k}_1)^2\}}{(2\pi)^{1/2} \sigma_u} F_i\{(\tilde{k} - \tilde{k}_0) / \tilde{k}_1; \theta_0\} \{1 + \Delta(\tilde{k})\}. \quad (16)$$

We can simplify the problem further by noting some facts about equation (16): the effect of the surface wave slopes is contained in the Gaussian probability function and it acts in essence as a Gaussian bandpass filter centered at \tilde{k}_0 of width $\sigma_u \tilde{k}_1$. From the literature and our *in situ* data (figure 1) we can expect $S(k)$ to present power law $\propto k^{-3}$ behavior and to vary slower over the range of the wavenumbers, k , than the Gaussian filter.

To the first order approximation, we can also assume that the effect of the local slope on the Fresnel coefficients can be neglected and that they will attain their value as for the nominal incidence θ_0 , i.e. $F_i(\theta_0) = F_i(s_x = 0; \theta_0) = F_i(s_x; \theta_0) = 16\pi^2 k_0^4 |g_i(\theta_0)|^2$. As before, we also assume that the spreading function $\Delta(k)$ is effectively constant over the wavenumber range sensed by QuikSCAT. With these assumptions we can re-write equation (16) as:

$$NRCS(\theta_0) \simeq \frac{2F_i(\theta_0)\{1 + \Delta(\tilde{k}_0)\}}{(2\pi)^{1/2} \sigma_u \tilde{k}_1} \int_0^\infty dk \frac{S(\tilde{k})}{k} \exp\{-(k - k_0)^2 / 2(\sigma_u k_1)^2\}. \quad (17)$$

To the leading order we can simplify equation (17) by observing that $S(k)$ can be effectively assumed to be zero outside the Gaussian bandpass filter centered at \tilde{k}_0 and of width $\delta = \sigma_u \tilde{k}_1$. To estimate the leading terms of equation (17), we expand under the integral equation (17) the Gaussian and $1/\tilde{k}$ term in a Taylor expansion around \tilde{k}_0 in radius of δ . We then obtain:

$$NRCS(\theta_0) \simeq \frac{2F_i(\theta_0)\{1 + \Delta(\tilde{k}_0)\}}{(2\pi)^{1/2} \delta \tilde{k}_0} \int_{\tilde{k}_0 - \delta}^{\tilde{k}_0 + \delta} dk S(k) \left\{ 1 - \frac{(k - \tilde{k}_0)^2}{2(\sigma_u \tilde{k}_1)^2} + O\{\sigma_u^2\} \right\}, \quad (18)$$

where the symbol $O()$ denotes the error of the approximation and $\sigma_u \ll 1$. For spectrum $S(k)$ following a power law, we can further simplify the integrand in equation (18) by noting:

$$\int_{\tilde{k}_0 - \delta}^{\tilde{k}_0 + \delta} dk S(k) (k - \tilde{k}_0)^2 \quad (19)$$

$$= \int_{\tilde{k}_0 - \delta}^{\tilde{k}_0 + \delta} dk S(k) \tilde{k}^2 - \tilde{k}_0^2 \int_{\tilde{k}_0 - \delta}^{\tilde{k}_0 + \delta} dk S(k) + \frac{4}{3} k_o \delta^2 S'(\tilde{k}_0) + O\{\sigma_u^2 L\} \quad (20)$$

$$\simeq \int_{\tilde{k}_0 - \delta}^{\tilde{k}_0 + \delta} dk S(k) \tilde{k}^2 - \tilde{k}_0^2 \int_{\tilde{k}_0 - \delta}^{\tilde{k}_0 + \delta} dk S(k) + \frac{4}{3} \tilde{k}_0 \delta^2 S'(\tilde{k}_0), \quad (21)$$

and substituting expressions (5) and (6) we get:

$$\int_{\tilde{k}_0 - \delta}^{\tilde{k}_0 + \delta} dk S(k) (k - \tilde{k}_0)^2 \simeq \langle mss \rangle_{\tilde{k}_0 - \delta}^{\tilde{k}_0 + \delta} - \tilde{k}_0^2 \langle \xi^2 \rangle_{\tilde{k}_0 - \delta}^{\tilde{k}_0 + \delta} + \frac{2}{3} \tilde{k}_0 \left\{ \langle \xi^2 \rangle_{\tilde{k}_0 - \delta}^{\tilde{k}_0} - \langle \xi^2 \rangle_{\tilde{k}_0}^{\tilde{k}_0 + \delta} \right\} \quad (22)$$

where $\langle \int_{\tilde{k}_0 - \delta}^{\tilde{k}_0 + \delta}$ denotes an integral over the QuikSCAT wavebands, i.e. $[\tilde{k}_0 - \sigma_u \tilde{k}_1, \tilde{k}_0 + \sigma_u \tilde{k}_1] = [\tilde{k}_0 - \delta, \tilde{k}_0 + \delta]$ so the $\langle mss \rangle_{\tilde{k}_0 - \delta}^{\tilde{k}_0 + \delta}$ is the mean slope as defined in equation (6) over the QuikSCAT wavebands and $\langle \xi^2 \rangle_{\tilde{k}_0 - \delta}^{\tilde{k}_0 + \delta}$ is the mean square surface displacement equation (5) over the QuikSCAT wavebands. In addition we note that for the relatively narrow waveband of surface waves contributing to the

Bragg signal we can relate $\langle mss \rangle$ to $\langle \zeta^2 \rangle$ as: $\langle mss \rangle \simeq \langle \zeta^2 \rangle \tilde{k}_0^2$. This is obtained via equation (6) and equation (5) after Taylor expanding them around $S(k_o)$ over the interval $[\tilde{k}_0 - \sigma_u \tilde{k}_1, \tilde{k}_0 + \sigma_u \tilde{k}_1]$.

During the GasEx2001 observations where the mean winds were relatively steady the QuikSCAT short waveband due to the long wave modulations were $([\tilde{k}_0 - \sigma_u \tilde{k}_1, \tilde{k}_0 + \sigma_u \tilde{k}_1])$: *h-pol* between 364 and 442 rad m⁻¹ and *v-pol* between 421 and 485 rad m⁻¹. After inserting equation (22) into the expression for the NRCS, equation (18), and retaining the most significant terms we get the final expression for the upwind NRCS:

$$NRCS(\theta_0) \simeq \frac{2F_i(\theta_0)\{1 + \Delta(\tilde{k}_0)\}}{(2\pi)^{1/2} \tilde{k}_0^3 \delta} \left\{ \langle mss \rangle_{\tilde{k}_0 - \delta}^{\tilde{k}_0 + \delta} + \frac{\tilde{k}_o}{3\delta} (\langle mss \rangle_{\tilde{k}_0 - \delta}^{\tilde{k}_0} - \langle mss \rangle_{\tilde{k}_0}^{\tilde{k}_0 + \delta}) \right\}. \quad (23)$$

Equation (23) has a simple physical interpretation: the upwind NRCS observed by QuikSCAT primarily depends on the short wave slopes $\langle mss \rangle_{\tilde{k}_0 - \delta}^{\tilde{k}_0 + \delta}$ and the difference between wave slopes within the QuikSCAT waveband or the local wave spectra slope $S'(k)$, equation (21).

If this difference, i.e. $\langle mss \rangle_{\tilde{k}_0 - \delta}^{\tilde{k}_0} - \langle mss \rangle_{\tilde{k}_0}^{\tilde{k}_0 + \delta}$ (due to, for example, changes of part of the short wave spectrum) varies significantly than its contribution will be reflected in the received NRCS values. The observed NRCS according to equation (23) is also modulated by the width of the probability distribution of the long wave slopes. This dependence on the long wave slope can be greatly reduced by using the ratio of $NRCS(\theta_{vv})/NRCS(\theta_{hh})$. The *in situ* wave slope spectra measured during GasEx 2001, $k^2 S(k)$, and the portion of wave slope spectra reflected in the NRCS signal of QuikSCAT are presented in figure 1.

We will denote the $\langle mss \rangle_{\tilde{k}_0 - \delta}^{\tilde{k}_0 + \delta}$ from within the QuikSCAT wavebands $[\tilde{k}_0 - \sigma_u \tilde{k}_1, \tilde{k}_0 + \sigma_u \tilde{k}_1]$ as mss_{12} where indexes 1 and 2 refer to lower/upper extent of the sensed wavebands. Neglecting the contribution of difference between wave slopes within the QuikSCAT waveband in equation (23) and expressing the relation between the upwind NRCS and the mss_{12} in decibels we get:

$$NRCS(\theta_0)(db) = \log(mss_{12}) + B(\theta_0) \quad (24)$$

where $B(\theta_0) = 2F_i(\theta_0)\{1 + \Delta(\tilde{k}_0)\}/\{(2\pi)^{1/2} \tilde{k}_0^3 \delta\}$ is a *polarization (v-pol and h-pol) and mean long wave slope dependent constant*. Based on this equation and recognizing that we have made numerous simplifying assumptions during the derivation of the equation equation (24) we propose the following relationship between the upwind NRCS and the mss_{12} as:

$$NRCS(\theta_0)(db) = A \log(mss_{12}) + B(\theta_0) \quad (25)$$

where A is a constant weakly dependent on polarization.